The Canadian Mineralogist
Vol. 46, pp. 1355-1364 (2008)
DOI: 10.3749/canmin.46.5.1355

A NEW CRYSTAL-CHEMICAL VARIATION OF THE ALUNITE-TYPE STRUCTURE IN MONOCLINIC $PbZn_{0.5}Fe_3(AsO_4)_2(OH)_6$

IAN E. GREY§ AND W. GUS MUMME

CSIRO Minerals, Box 312, Clayton South, Victoria, 3169, Australia

PIERRE BORDET

CNRS, Institut Neel, BP 166, F–38042 Grenoble, France

STUART J. MILLS

Department of Earth and Ocean Sciences, University of British Columbia, Vancouver, British Columbia V6T 1Z4, Canada

ABSTRACT

The crystal structure of a segnitite-related mineral with composition $Pb[Zn_{0.5}\square_{0.5}]Fe_3(AsO_4)_2(OH)_6$, $\square$ = vacancy, from Broken Hill, Australia, has been determined using single-crystal X-ray data. The mineral has monoclinic symmetry, space group $C2/c$, with a 25.8898(6), b 14.8753(2), c 12.1700(2) Å, β 110.681(1)°, Z = 16. All crystals examined were found to be multiply twinned by 120° rotations about c^*, which corresponds with c_h of the hexagonal alunite-type subcell. The structure was determined on a twinned crystal with one dominant individual, and refined to R = 0.055 for 4089 reflections with $F > 4\sigma F$. The general features of the monoclinic structure match those of the prototype rhombohedral alunite-type structure. This involves a rhombohedral stacking of hexagonal tungsten-bronze-type sheets of corner-connected octahedra that share their apical anions with AsO_4 tetrahedra on either side of the layer of octahedra, with Pb atoms located between the layers. However, the structure differs from those of other alunite-type minerals in having zinc atoms ordered in trigonal bipyramidal sites in half of the available six-membered rings of the layers of octahedra. These sites are unoccupied in previously reported alunite-type structures. Ordered displacements of the Pb atoms occur in response to the Zn–$\square$ ordering.

Keywords: lead iron zinc hydroxyarsenate, crystal structure, alunite-type monoclinic superstructure, composition and displacement modulation.

SOMMAIRE

Nous avons déterminé la structure cristalline d'un minéral semblable à la ségnitite ayant la composition $Pb[Zn_{0.5}\square_{0.5}]Fe_3(AsO_4)_2(OH)_6$, $\square$ signifiant une lacune, provenant de Broken Hill, en Australie, par diffraction X sur monocristal. Le minéral possède une symétrie monoclinique, groupe spatial $C2/c$, avec a 25.8898(6), b 14.8753(2), c 12.1700(2) Å, β 110.681(1)°, Z = 16. Tous les cristaux que nous avons examinés sont maclés de façon multiple par rotations de 120° autour de c^*, ce qui correspond à c_h d'une sous-maille hexagonale de type alunite. Nous nous sommes servis d'un cristal maclé contenant un individu prédominant, et nous l'avons affiné jusqu'à un résidu R de 0.055 pour 4089 réflexions ayant $F > 4\sigma F$. Les aspects généraux de la structure monoclinique concordent avec ceux de la structure rhomboédrique prototypique. Par exemple, il y a un empilement rhomboédrique de feuillets hexagonaux de type bronze tungstique impliquant des octaèdres à coins partagés avec des tétraèdres AsO_4 de chaque côté des couches d'octaèdres, les atomes de Pb étant situés entre les couches. Toutefois, la structure se distingue de celle des autres minéraux du supergroupe de l'alunite en ayant des atomes de zinc mis en ordre dans des sites bipyramidaux trigonaux dans la moitié des sites disponibles dans les anneaux à six membres des couches d'octaèdres. Ces sites demeurent vacants dans les structures décrites antérieurement. Des déplacements ordonnés des atomes de Pb résultent d'une mise en ordre des atomes de Zn et des lacunes.

(Traduit par la Rédaction)

Mots-clés: hydroxyarsenate de plomb, fer et zinc, structure cristalline, surstructure monoclinique de type alunite, modulation de composition et de déplacements.

§ *E-mail address*: ian.grey@csiro.au

Introduction

Segnitite, $PbFe_3H(AsO_4)_2(OH)_6$, from Broken Hill, New South Wales, was described and approved as a new mineral in 1992 (Birch *et al.* 1992). It is a member of the alunite–jarosite supergroup, with the general formula $DG_3(TO_4)_2(OH,H_2O)_6$, where *D* represents large cations such as Na^+, K^+, H_3O^+,Ba^{2+}, Sr^{2+}, Ca^{2+}, Pb^{2+}, REE^{3+}; *G* is an octahedral site containing typically Al^{3+} or Fe^{3+}, but it can also include V^{3+}, Ga^{3+}, Zn^{2+} and Cu^{2+}. The tetrahedral site *T* is occupied by S, P or As (Scott 1987, Jambor 1999). Most alunite-related minerals have a rhombohedral symmetry, $R\bar{3}m$, with cell parameters $a_h \simeq 7$ Å, $c_h \simeq 17$ Å (Menchetti & Sabelli 1976). The structure is based on a rhombohedral stacking of composite (001) layers of octahedra and tetrahedra, with the *D* cations packing between the layers. The composite layers comprise hexagonal tungsten-bronze-type sheets of corner-connected octahedra that share their apical anions with TO_4 tetrahedra on either side of the layer of octahedra.

Segnitite is a secondary mineral derived from the breakdown of primary sulfide ores containing minerals such as galena, sphalerite, chalcopyrite and arsenopyrite (van der Heyden & Edgecombe 1990). In the oxidized zone of the Broken Hill orebody, it forms extensive solid-solutions with sulfate and phosphate end-members (Rattray *et al.* 1996). During a general study of segnitite-related minerals from Broken Hill (Mills 2007), we encountered crystals having a segnitite-like composition but with an X-ray-diffraction pattern displaying a departure from rhombohedral symmetry and the presence of superlattice reflections requiring a doubling of each of the axes of the pseudohexagonal cell. The mineral was found to have monoclinic symmetry, *C2/c*, with $a = 2\sqrt{3}a_h = 25.8898(2)$ Å, $b = 2b_h = 14.8753(2)$ Å, $c = 1/3[\sqrt{3}a_h + c_h] = 12.1700(2)$ Å, $\beta = 110.681(1)°$. The crystals are all twinned by 120° rotation about the pseudohexagonal c_h axis, but a crystal was eventually found that has one dominant twin individual. It was used for a structure determination, the results of which are reported here.

Experimental

Occurrence and chemical composition

Analyzed crystals of the mineral are from a single small cavity in a hand specimen from the Kintore open-cut mine at Broken Hill. Birch & van der Heyden (1997) have described in detail the location of various oxidized zones and mineral assemblages at the Kintore open cut. The hand specimen was taken from the footwall of number 3 ore lens between 230 and 240 meters (above sea level) near the base of the pit at the southern end (shown in Fig. 7 of Birch & van der Heyden 1997). Clusters of platy crystals, up to 0.5 mm in largest dimension, grow out from, and are intergrown with, bright red grains of another lead iron hydroxy arsenate, carminite, $PbFe_2(AsO_4)_2(OH)_2$ (Foshag 1937). The crystals are lemon yellow in color and readily distinguished from greenish brown to yellowish brown crystals of normal rhombohedral segnitite, present in other cavities of the same specimen.

Sectioned and polished crystals were examined with a scanning electron microscope using a back-scattered electron (BSE) detector. Zoning, as shown by slight variations in BSE contrast, was found to be due to small variations (1 to 3 wt%) in zinc content over regions of the order of tens of micrometers. The crystals were analyzed using a JEOL Superprobe operated in wavelength-dispersion mode at an accelerating voltage of 15 kV and a current of 20 nA. The low voltage used, together with the use of a light-element detector, allowed the sample to be analyzed directly for oxygen. We used the standards anglesite, $PbSO_4$, for Pb ($M\alpha$ line), S ($K\alpha$) and O ($K\alpha$), $MgAl_2O_4$ for Al ($K\alpha$), chalcopyrite, $CuFeS_2$ for Cu ($K\alpha$), hematite, Fe_2O_3 for Fe ($K\alpha$), apatite, $Ca_5(PO_4)_3OH$ for P ($K\alpha$), ZnS for Zn ($L\alpha$) and GaAs for As ($L\alpha$). The beam was defocused to 10 μm for the analyses.

The analytical method was tested by analysis of the coexisting carminite. The average of five analyses of carminite crystals gave $PbFe_{1.96}Zn_{0.03}Al_{0.01}As_{1.99}P_{0.01}O_8(OH)_{2.03}$, in close accord with its ideal formula. The results of the electron-microprobe analyses of the monoclinic mineral, together with those of associated carminite and for rhombohedral segnitite from the same hand specimen, are reported in Table 1. The empirical formula, normalized to 14 anions and charge-balanced is $Pb_{0.99}Zn_{0.26}Cu_{0.03}Fe_{3.06}Al_{0.03}(AsO_4)_{2.05}(SO_4)_{0.06}(OH)_{5.56}$. The ideal formula is $PbZn_{0.5}Fe_3(AsO_4)_2(OH)_6$.

X-ray diffraction and evidence of twinning

Diffraction patterns obtained for $PbZn_{0.5}Fe_3(AsO_4)_2(OH)_6$ using a precession camera have a close resem-

TABLE 1. RESULTS OF ELECTRON-MICROPROBE ANALYSES

Consituent	Monoclinic $PbZn_{0.5}Fe_3(AsO_4)_2(OH)_6$ *		Rhombohedral segnitite	Carminite
	Average	Range		
Pb wt.%	26.06	25.11 to 27.49	27.41	33.38
Fe	21.63	21.07 to 22.22	21.97	17.65
Zn	2.19	1.77 to 2.52	0.42	0.29
Cu	0.27	0.12 to 0.43	0.11	0.00
Al	0.11	0.10 to 0.18	0.28	0.05
As	19.46	18.70 to 20.17	16.68	24.04
S	0.25	0.15 to 0.60	1.73	0.01
P	0.02	0.02 to 0.04	0.01	0.02
O	30.42	30.05 to 30.70	31.66	26.76
Total	100.40	99.1 to 102.1	100.29	102.13

* Average result of 10 analyses.

blance to those for rhombohedral segnitite, with the strong reflections all indexable using a hexagonal cell with a_h = 7.45 Å, c_h = 17.1 Å. However, the intensities are not consistent with trigonal symmetry, and longer-exposure photographs show extra spots aligned parallel to the reciprocal rhombohedral axes (≡ <101>$_h$*), requiring a doubling of all three axes. Examination of the intensities of the superlattice reflections in the precession patterns from various crystals showed that the relative intensities of equivalent reflections along each of the a^*_{rhomb} axes vary considerably from crystal to crystal, suggesting that twinning is present. Crystals free of twinning could not be found. However, one of the crystals was found to have intensities of superlattice reflections along one reciprocal rhombohedral axis of the order of six times stronger than those along the other two axes. This crystal was used for the structure analysis.

The crystal with one dominant twin individual was mounted on a Nonius Kappa CCD diffractometer for collection of intensity data. Data-collection conditions are given in Table 2. Indexing of the full dataset using a pseudohexagonal cell required a doubling of a_h and b_h, and a quadrupling of c_h. The strongest 4 × c_h reflections have intensities that are only one fifth those of the superlattice reflections along <101>$_h$*. Subsequent analysis showed that the quadrupling of c_h is only apparent, due to the juxtaposition of reflections from the different twin individuals. The full dataset was indexed with a primitive triclinic cell having *a* 14.8753(2), *b* 14.9299(2), *c* 24.3401(4) Å, α 72.1818(5), β 90.0245(6), γ 60.117(2)°. The pseudohexagonal subcell parameters can be derived from these parameters by applying the matrix (0 ½ 0, $\overline{½}$ 0 0, ¼ $\overline{½}$ ¾). A careful inspection of the precession photographs, indexed using the triclinic cell, showed that halving of the *c* axis to 12.17 Å resulted in elimination of the superlattice reflections from the two minor twin-domains, while leaving intact the superlattice reflections from the dominant twin-domain, and the 4 × c_h type reflections. The structure determination was then conducted using the triclinic dataset with a *c* of 12.17 Å. In the course of the structure determination, the true symmetry was found to be monoclinic.

TABLE 2. DATA COLLECTION AND REFINEMENT INFORMATION FOR MONOCLINIC $PbZn_{0.5}Fe_3(AsO_4)_2(OH)_6$

Ideal formula		$Pb[Zn_{0.5}\square_{0.5}]Fe_3(AsO_4)_2(OH)_6$			
Data for twinned crystal in triclinic cell					
Unit-cell parameters					
a (Å)	14.8753(2)	*b* (Å)	14.9299(2)	*c* (Å)	24.3401(4)
α (°)	72.1818(5)	β (°)	90.0245(6)	γ (°)	60.117(1)
V (Å^3)	4384.9	*Z*	16		
Space group			$P\overline{1}$		
Radiation			MoKα		
Crystal shape and size (mm)			Lath, 0.03 × 0.06 × 0.15		
Collection mode			φ scan 0-360°, Δφ = 0.5° plus five ω scans		
Count time per frame (s)			60		
Maximum 2θ (°)			56.6		
Completeness of data			97.6%		
Total number of reflections			71397		
Number of unique reflections			21071		
Absorption correction			SADABS, μ = 26.3 mm^{-1}		
T_{min}/T_{max}			0.57		
R_{merge}			0.074		
Data for dominant twin individual, monoclinic symmetry					
Unit-cell parameters					
a (Å)	25.8898(6)	*b* (Å)	14.8753(2)	*c* (Å)	12.1700(2)
β (°)	110.681(1)	*V* (Å^3)	4384.9	*Z*	16
Space group			*C2/c*		
Number of unique reflections			5340		
Number of observed reflections, $F > 4\sigma F$			4089		
Refinement in *C2/c*					
Number of parameters refined			264		
Refined volume-fractions of twin			0.702(3), 0.148(2), 0.150(2)		
R, $F > 4\sigma F$			0.055		
R, all reflections			0.077		
wR (F^2) all reflections			0.091		
GOF			1.19		
$\Delta\sigma_{min}$, $\Delta\sigma_{max}$ (e/Å^3)			-1.8, +1.9 (adjacent to Pb1)		

Structure determination and refinement

The first stage of the structure determination was an analysis of the average structure based on the pseudohexagonal subcell reflections only. This type of preliminary study can be useful in indicating the perturbations of the parent rhombohedral structure responsible for the weaker superlattice reflections (Grey *et al*. 2003*a*). Transformation of the triclinic dataset to the 7.45 × 7.45 × 17.1 hexagonal cell and merging in $R\overline{3}m$ gave a high R_{merg} of 0.14. The atom coordinates for rhombohedral segnitite (Mills 2007) were used in a SHELX (Sheldrick 1997) refinement using isotropic atomic displacement parameters (ADPs), giving R_1 = 0.08. The framework atoms (Fe, As, O) showed almost no deviation from their positions in rhombohedral segnitite and had small displacement parameters. In contrast, the Pb atom was split between sites displaced along <1$\overline{1}$0>$_h$ directions by 0.5 Å from the ideal site at 0,0,0 and had an elevated isotropic displacement parameter. In addition, a difference-Fourier map showed the partial occupancy of new metal atom sites lying in the plane of the hexagonal rings of the layers of octahedra, and displaced by ~0.8 Å from the centers of the rings. These atoms have three distances of 2.0–2.4 Å to oxygen atoms forming the rings, and two shorter distances of 1.7 and 1.8 Å to oxygen atoms above and below the rings. Subsequent bond-valence analyses indicated that zinc atoms are ordered at these five-coordinated sites.

The analysis was then directed to the data for the triclinic cell, with the *c* axis halved to 12.17 Å as given in the preceding section. The positions of the Pb, As, and Fe atoms in the triclinic cell, $P\overline{1}$, were located using direct methods (Farrugia 1999). The oxygen atoms and the five-coordinated metal atoms were located in successive difference-Fourier maps. The refinements using SHELX–97 of all coordinates and isotropic displacement parameters converged at R_1 = 0.105 for 7124 observed reflections. Refinement of anisotropic ADPs for the metal atoms reduced R_1 to

0.083. However, the refined model involved multiply split lead atoms at each of the four crystallographically independent sites. As discussed by Bindi & Evain (2007), this type of situation is generally better modeled using non-harmonic ADPs, which can involve a smaller number of refined parameters and much lower correlations between the refined parameters. Accordingly, we changed to the JANA 2000 program suite (Petříček & Dušek 2000), which incorporates non-harmonic ADPs based on the Gram–Charlier expansion of the structure factors (Kuhs 1992, Trueblood *et al.* 1996). Each of the clusters of split lead atoms was replaced with a single lead atom, and the third-order non-harmonic ADPs for the lead atoms were refined using JANA 2000. Anisotropic displacement parameters were employed for the other metal atoms. The five-coordinated sites were split between pairs of sites on opposite sides of the hexagonal rings in the layers of octahedra, separated by ~1.6 Å. The site occupancies of these pairs of partially occupied sites were refined. A correction for twinning by rotation about c^* ($\equiv c_h$) by 120° and 240° was also conducted. The refinement converged smoothly to $R = 0.062$.

The possibility of higher symmetry was checked by applying PLATON/ADDSYM (Spek 2003) to the $P\bar{1}$ structure model. The analysis showed that the structure can be described using the monoclinic space-group $C2/c$, after applying the transformation matrix ($\bar{1}$ 2 0, 1 0 0, 0 0 $\bar{1}$) and shifting the origin to (¼,¼,0). The transformed cell has a 25.8898(6), b 14.8753(2), c 12.1700(2) Å, β 110.681(1)°. The coordinates and ADPs of the atoms were transformed, and the structure was then refined in $C2/c$ using JANA 2000. Refinement of all coordinates, ADPs and occupancy of the five-coordinated site converged at $R = 0.055$. Refinement details are given in Table 2. The refined coordinates and equivalent isotropic displacement parameters are reported in Table 3. The anisotropic displacement parameters for the Pb and Zn atoms as well as the anharmonic displacement parameters for the Pb atoms are reported in Table 4. The anisotropic displacement parameters for the As and Fe atoms show only small departures from isotropic character. Tables of observed and calculated structure-factors are available from the Depository of Unpublished Data on the MAC website [document "Segnitite"-Like Mineral CM46_1355].

DESCRIPTION OF THE STRUCTURE

The general structural features of monoclinic $PbZn_{0.5}Fe_3(AsO_4)_2(OH)_6$ closely match those of the prototype structure of rhombohedral alunite (Menchetti & Sabelli 1976). The $Fe^{3+}(OH)_4O_2$ octahedra corner-connect *via* the OH anions to form hexagonal tungsten-bronze-type sheets of three- and six-membered rings. The octahedra are tilted such that the apical atoms of oxygen on one side of each three-membered ring are shared with AsO_4 tetrahedra, forming composite layers as shown in Figure 1. The presence of twinning, together with the presence of the strong absorber Pb, prevented the experimental location of the H atoms of the $Fe(OH)_4O_2$ groups. The labeling of anions #17 to #28 as OH in Table 3 is consistent with the well-established crystal chemistry of alunite-related structures.

In alunite-related structures, the composite layers of corner-shared octahedra and tetrahedra shown in Figure 1 are stacked along the c_h axis, with offsets corresponding to the rhombohedral translation vectors $\pm[^1/_3,^2/_3,^2/_3]_h$. The rhombohedral stacking of the layers gives rise to the interlayer 12-coordinated D sites along the c_h axis, as shown in Figure 2a. As shown in this diagram, three-membered rings of octahedra in adjacent layers about the origin are in an eclipsed relationship, and the large D cation (Pb^{2+} in segnitite) is located at the center of gravity of the six octahedra. This provides icosahedral coordination to six apical oxygen atoms and six equatorial hydroxyl anions (Fig. 2a) of the octahedra at distances of ~2.9 Å and 2.8 Å, respectively. In monoclinic $PbZn_{0.5}Fe_3(AsO_4)_2(OH)_6$, the Pb

TABLE 3. ATOMIC COORDINATES AND EQUIVALENT ISOTROPIC DISPLACEMENT PARAMETERS (Å²) FOR MONOCLINIC $PbZn_{0.5}Fe_3(AsO_4)_2(OH)_6$

Atom	*x*	*y*	*z*	U_{eq}
Pb1	0.61159(8)	0.1142(1)	0.9955(1)	0.0400(3)
Pb2	0.60614(8)	0.63451(9)	0.0035(1)	0.0334(3)
Zn1	0.78368(9)	0.8724(1)	0.2570(2)	0.0205(9)
Zn2	0.7158(5)	0.876(1)	0.243(1)	0.055(6)
As1	0.04625(5)	0.37548(6)	0.0273(1)	0.0067(4)
As2	0.70550(6)	0.37440(7)	0.9649(1)	0.0091(4)
As3	0.29788(6)	0.12454(7)	0.0308(1)	0.0088(4)
As4	0.04865(5)	0.87495(7)	0.0293(1)	0.0074(4)
Fe1	0.74873(7)	0.6247(1)	0.2430(1)	0.0121(8)
Fe2	0.62168(7)	0.4972(1)	0.7547(1)	0.0077(6)
Fe3	0	0.1242(1)	0.75	0.0068(8)
Fe4	0	0.3743(1)	0.25	0.0067(8)
Fe5	0.37592(7)	0.7508(1)	0.2429(1)	0.0081(6)
Fe6	0.12343(7)	0.5010(1)	0.2524(1)	0.0071(6)
Fe7	0.87789(7)	0.7467(1)	0.2473(1)	0.0089(6)
O1	0.0212(4)	0.3744(4)	0.8836(7)	0.007(2)
O2	0.4937(4)	0.1237(5)	0.5801(8)	0.009(2)
O3	0.4146(3)	0.7824(5)	0.4162(7)	0.010(2)
O4	0.9131(4)	0.5328(5)	0.9164(7)	0.010(2)
O5	0.2651(4)	0.3757(5)	0.3902(8)	0.019(2)
O6	0.7435(4)	0.8748(5)	0.5883(9)	0.013(2)
O7	0.8348(3)	0.7822(5)	0.5791(7)	0.009(2)
O8	0.8355(4)	0.9672(5)	0.5801(7)	0.013(2)
O9	0.7227(5)	0.8750(5)	0.1151(9)	0.027(2)
O10	0.8370(4)	0.4682(5)	0.5798(7)	0.010(2)
O11	0.7432(4)	0.3757(5)	0.5766(8)	0.012(2)
O12	0.3369(3)	0.2180(5)	0.0812(7)	0.010(2)
O13	0.9761(4)	0.1253(4)	0.1148(7)	0.010(2)
O14	0.0875(4)	0.0315(5)	0.5853(7)	0.011(2)
O15	0.0890(4)	0.2159(5)	0.5854(7)	0.010(2)
O16	0.9953(4)	0.1272(5)	0.5818(8)	0.009(2)
OH17	0.3129(4)	0.7169(5)	0.2983(7)	0.011(2)
OH18	0.1885(4)	0.5331(6)	0.2063(7)	0.012(2)
OH19	0.1895(4)	0.0252(5)	0.2009(7)	0.011(2)
OH20	0.3079(4)	0.2263(5)	0.2886(7)	0.011(2)
OH21	0.0589(3)	0.9713(5)	0.3019(7)	0.006(1)
OH22	0.5914(4)	0.3740(4)	0.7051(8)	0.007(2)
OH23	0.1534(4)	0.1256(5)	0.8014(9)	0.015(2)
OH24	0.9413(3)	0.2199(5)	0.6993(7)	0.007(2)
OH25	0.9400(3)	0.2808(5)	0.1980(7)	0.007(2)
OH26	0.0595(3)	0.4711(5)	0.3004(7)	0.007(2)
OH27	0.8490(4)	0.6250(5)	0.7029(9)	0.012(2)
OH28	0.0924(4)	0.6244(4)	0.2032(8)	0.007(2)

* Site occupancies of Zn1 and Zn2 are 0.700(8) and 0.177(9).
** All atoms in general site 8(f) except for Fe3 and Fe4, in site 4(e).

TABLE 4. ANISOTROPIC (Å^2) AND ANHARMONIC DISPLACEMENT PARAMETERS FOR Pb AND Zn ATOMS IN MONOCLINIC $PbZn_{0.5}Fe_3(AsO_4)_2(OH)_6$

	Pb1	Pb2	Zn1	Zn2		Pb1	Pb2
U_{11}	0.0325(4)	0.0246(5)	0.009(1)	0.016(6)	C_{111}*	0.00024(2)	0.00033(2)
U_{22}	0.0635(7)	0.0520(6)	0.047(2)	0.13(1)	C_{112}	0.00009(2)	-0.00012(2)
U_{33}	0.0181(3)	0.0185(3)	0.007(1)	0.012(6)	C_{113}	0.00021(3)	-0.00014(2)
U_{12}	-0.0124(3)	-0.0020(3)	0.0011(8)	0.002(6)	C_{122}	0.00007(5)	0.00074(4)
U_{13}	0.0018(3)	0.0011(3)	0.0038(9)	0.002(5)	C_{123}	-0.00014(3)	0.00012(3)
U_{23}	0.0033(3)	0.0026(3)	0.0001(9)	0.009(6)	C_{133}	-0.00008(6)	0.00035(5)
					C_{222}	0.0060(2)	-0.0038(1)
					C_{223}	0.00068(9)	-0.00087(8)
					C_{233}	0.00049(9)	-0.00062(8)
					C_{333}	0.0008(2)	-0.0015(2)

* The C_{ijk} are multiplied by 10^3.

TABLE 5. INTERATOMIC DISTANCES IN MONOCLINIC $PbZn_{0.5}Fe_3(AsO_4)_2(OH)_6$

M-O	Distance (Å)	*M*-O	Distance (Å)
Pb1-O2	2.55(1)	Pb2-O3	2.541(9)
Pb1-O4	2.612(9)	Pb2-O14	2.768(9)
Pb1-O10	2.862(9)	Pb2-O16	2.462(9)
Pb1-O15	2.894(9)	Pb2-OH17	2.853(8)
Pb1-OH18	2.897(8)	Pb2-OH21	2.806(7)
Pb1-OH25	2.747(8)	Pb2-OH22	2.62(1)
Pb1-OH26	2.609(7)	Pb2-OH24	2.659(8)
Pb1-OH27	2.94(1)		
Pb1-OH28	2.75(1)		
Zn1-O5	1.85(1)	Zn2-O5	1.80(1)
Zn1-O9	1.88(1)	Zn2-O9	1.62(2)
Zn1-OH19	2.380(8)	Zn2-OH17	2.48(2)
Zn1-OH20	2.256(8)	Zn2-OH18	2.43(2)
Zn1-OH23	2.00(1)	Zn2-OH27	2.01(2)
As1-O1	1.637(8)	As2-O5	1.656(9)
As1-O2	1.70(1)	As2-O6	1.66(1)
As1-O3	1.710(8)	As2-O7	1.692(8)
As1-O4	1.712(8)	As2-O8	1.709(8)
As3-O9	1.664(1)	As4-O13	1.642(9)
As3-O10	1.690(8)	As4-O14	1.711(8)
As3-O11	1.69(1)	As4-O15	1.697(8)
As3-O12	1.701(8)	As4-O16	1.71(1)
Fe1-O6	1.99(1)	Fe2-O8	1.973(8)
Fe1-O11	1.98(1)	Fe2-O14	2.002(8)
Fe1-OH17	2.028(9)	Fe2-OH19	2.10(1)
Fe1-OH18	2.042(9)	Fe2-OH21	1.96(1)
Fe1-OH19	2.062(9)	Fe2-OH22	2.001(7)
Fe1-OH20	2.083(8)	Fe2-OH23	2.078(8)
Fe3-O16 ×2	2.01(1)	Fe4-O2 ×2	2.02(1)
Fe3-OH21 ×2	2.015(8)	Fe4-OH25 ×2	2.013(8)
Fe3-OH24 ×2	2.013(8)	Fe4-OH26 ×2	2.037(8)
Fe5-O3	2.045(8)	Fe6-O4	1.999(8)
Fe5-O7	1.962(8)	Fe6-O10	1.988(8)
Fe5-OH17	2.04(1)	Fe6-OH18	2.01(1)
Fe5-OH22	2.045(7)	Fe6-OH26	1.99(1)
Fe5-OH25	1.97(1)	Fe6-OH27	2.012(7)
Fe5-OH27	1.974(7)	Fe6-OH28	2.008(7)
Fe7-O12	1.969(8)	Fe7-OH23	2.067(8)
Fe7-O15	1.990(8)	Fe7-OH24	1.99(1)
Fe7-OH20	2.07(1)	Fe7-OH28	1.984(7)

atoms are displaced by ~0.5 Å from the centers of the icosahedra, resulting in lower coordination with nine Pb1–O less than 3 Å and seven Pb2–O less than 3 Å, as shown in Table 5.

The rhombohedral stacking of the composite layers of octahedra and tetrahedra in alunite-type structures results in the apices of the TO_4 tetrahedra being located directly above and below the centers of the six-membered rings of octahedra in adjacent layers of octahedra, as shown in Figure 2a. An atom located at the center of the ring would have 6 + 2 hexagonal bipyramidal coordination. The occupation of such sites had not previously been reported for alunite-type minerals. In monoclinic $PbZn_{0.5}Fe_3(AsO_4)_2(OH)_6$, Zn atoms occupy sites within the six-membered rings. They are displaced by ~0.8 Å from the centers of the rings toward one of the six equatorial OH anions, thereby establishing trigonal bipyramidal coordination. As seen from Table 5, the Zn atoms have two short bonds to the apices of the AsO_4 tetrahedra, with Zn–O in the range 1.62–1.88 Å, and three longer bonds in the range 2.00 to 2.48 Å to equatorial OH anions. The hexagonal bipyramids can be divided into six such five-coordinated sites, but only two of these sites are occupied, corresponding to displacements along ±[100]. One of these sites, Zn1, is dominant, with 70% occupancy, whereas the Zn2 site has only 18% occupancy.

A projection of the refined structure of monoclinic $PbZn_{0.5}Fe_3(AsO_4)_2(OH)_6$ along [010], showing the stacking of three composite layers, is shown in Figure 3. The Zn and Pb atoms are labeled. Only half of the six-membered rings in the layers of octahedra have zinc atoms located within them. This is more clearly illustrated in Figure 4, in which the structure is viewed along the direction of the pseudorhombohedral stacking vector. In this representation, the six-membered rings from successive layers of octahedra are aligned, giving channels normal to the plane of projection. Channels in successive (100) planes are alternately occupied and unoccupied by Zn atoms. In addition to this compositional modulation, there is a positional modulation of the Zn atoms in the occupied channels that lie within the same (100) plane. This is shown by the zig-zag positions of the Zn1 (and Zn2) atoms in successive occupied channels within the same (100) plane in Figure 4.

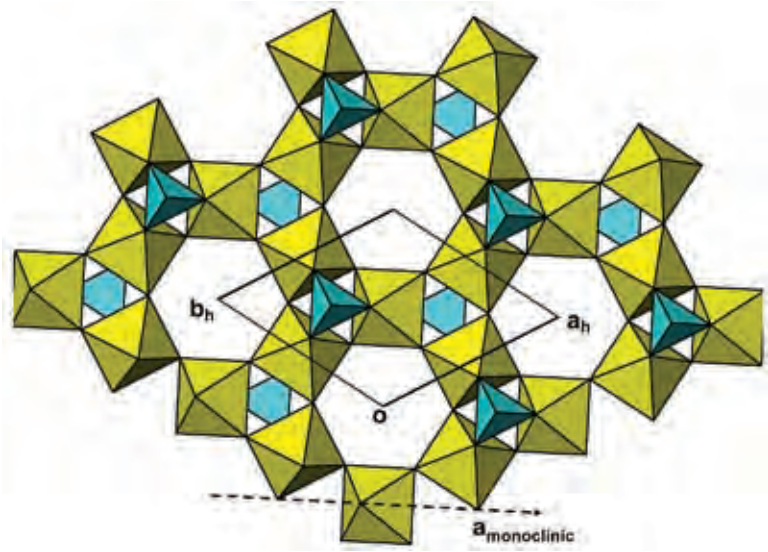

FIG. 1. Composite layer of corner-connected octahedra and tetrahedra that forms the fundamental building block in alunite-related structures, viewed parallel to c_h.

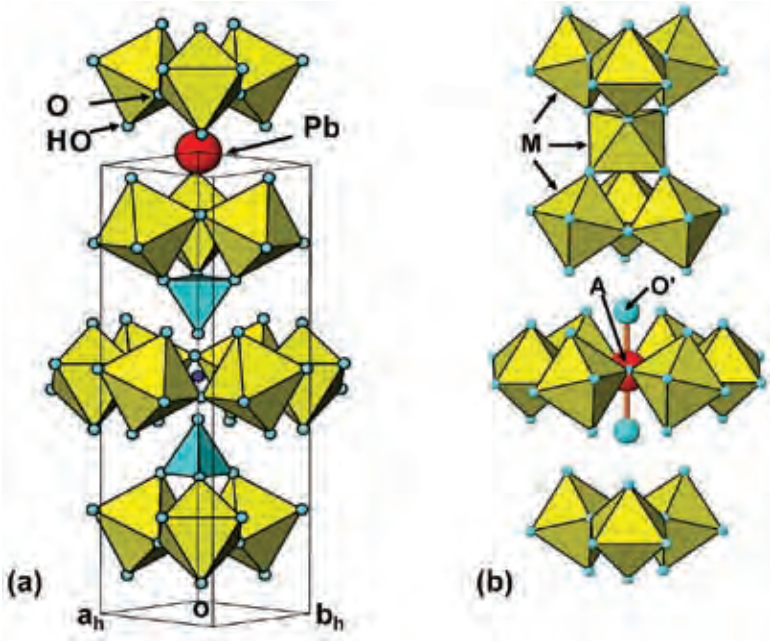

FIG. 2. Arrangement of polyhedra and atoms about the c_h axis in (a) the alunite-type structure and (b) in the pyrochlore-type structure.

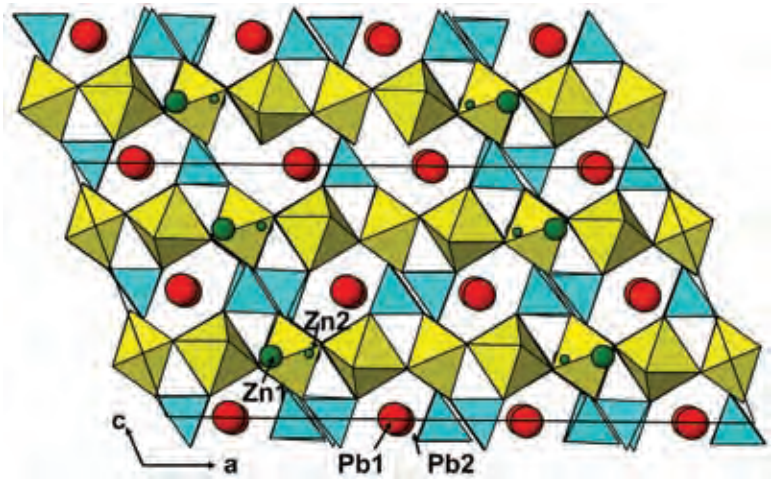

FIG. 3. Projection of the structure of monoclinic $PbZn_{0.5}Fe_3(AsO_4)_2(OH)_6$ along [010]. The Pb and Zn atoms are labeled.

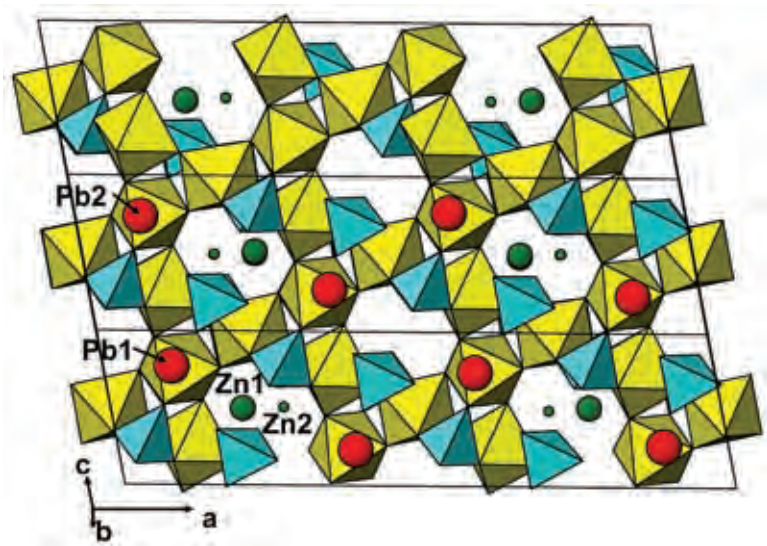

FIG. 4. The structure of monoclinic $PbZn_{0.5}Fe_3(AsO_4)_2(OH)_6$, viewed after a 30° rotation about the *a* axis from the [001] projection. The Pb and Zn atoms are labeled.

Figure 4 shows that there is a coupling between the displacements of the Pb atoms and the pattern of Zn ordering. The directions of the Pb displacements are readily identified by noting the positions of the Pb atoms relative to the upper triangular faces of the octahedra located directly below the Pb atoms in Figure 4. An undisplaced Pb atom at the center of the icosahedral site is located centrally above the triangular face of the octahedron. One can see that the displacements of the Pb1 and Pb2 atoms are away from the Zn-occupied channels and toward the unoccupied channels. The coupled compositional modulation of Zn atoms and Pb displacements gives rise to the subset of strong superlattice reflections oriented along $<101>_h^*$ of the pseudohexagonal subcell (see Experimental section) that require a doubling of both a_h and c_h. The displacement

modulation of the Zn atoms is essentially independent of the Pb displacements and is manifested by a weaker subset of superlattice reflections, requiring a doubling of the b_h axis of the pseudohexagonal cell. The indexing of these reflections in diffraction patterns for the twinned crystals also required a quadrupling of c_h. The structure analysis, however, shows that the apparent quadrupling of the c_h axis is due to the juxtaposition of reflections from different twin-related domains.

Discussion

Numerous single-crystal studies have been undertaken on alunite-related minerals (Jambor 1999). In the majority of cases, the cell geometry and space group conform to those of the prototype structure, with $a_h \approx 7$ Å, $c_h \approx 17$ Å, space group = $R\bar{3}m$. In the few cases where deviations occur, they are attributed to ordering of *D* cations and vacancies, giving a doubling of c_h, as for plumbojarosite, $Pb_{0.5}Fe_3(SO_4)_2(OH)_6$ (Szymański 1985), or to ordering of two different tetrahedrally coordinated *T* atoms, giving a lowering of the symmetry to *R*3*m* (Jambor *et al*. 1996). Radoslovich (1982) reported that the symmetry of gorceixite, $BaAl_3[PO_3(O,OH)]_2(OH)_6$, is lowered to orthorhombic, *Cm*, by ordered protonation of one of the two PO_4 groups. However, a recent single-crystal study on gorceixite from a different locality (Dzikowski *et al*. 2006) gave a better refinement in $R\bar{3}m$.

Monoclinic $PbZn_{0.5}Fe_3(AsO_4)_2(OH)_6$ is unique amongst the alunite-related minerals in having a new crystallographic site occupied in the structure. No previously reported alunite-type structure has occupation of sites within the six-membered rings of octahedra in the layers. However, other mineral structures containing hexagonal tungsten-bronze-type layers are known to incorporate small cations in off-center sites in the six-membered rings. The best known of these are the polytypes of zirconolite (Gatehouse *et al*. 1981, Coelho *et al*. 1997, Grey *et al*. 2003*b*) and the closely related zirkelite and "polymignyte" minerals (Mazzi & Munno 1983). In zirconolite, three quarters of the Ti atoms form the layers of octahedra, whereas the remaining one quarter of the Ti atoms is located in the six-membered rings. As for the case of Zn in monoclinic $PbZn_{0.5}Fe_3(AsO_4)_2(OH)_6$, the Ti atoms are displaced from the ring centers to adopt a distorted trigonal bipyramidal coordination. In the case of zirkelite and "polymignyte", the displaced atoms are Fe rather than Ti. In "polymignyte", the Fe atoms are displaced toward O–O edges of octahedra rather than individual O atoms forming the rings, giving tetrahedral rather than trigonal bipyramidal coordination (Mazzi & Munno 1983).

Pyrochlore, $A_2M_2O_6X$, is another mineral having occupation of six-membered rings in hexagonal tungsten-bronze-type layers. The extensive pyrochlore group of minerals have structures closely related to that of zirconolite (Mazzi & Munno 1983). Their cubic structures are based on stacking of hexagonal tungsten-bronze-type layers along the four equivalent three-fold axes = $<111>_{prc}$. Goreaud & Raveau (1980) have described the close relationship between pyrochlore-type and alunite-type structures. This is illustrated in Figure 2, in which the stacking of layers of octahedra along the three-fold (or pseudo three-fold) axes is seen to be the same in segnitite (Fig. 2a) and in pyrochlore (Fig. 2b). However, the two structure types have opposite senses of the tilting of the octahedra in the layers, and this affects how the other components are incorporated. In particular, the outward tilting of apices of octahedra in adjacent three-membered rings in alunite provides icosahedral sites for the large cations (Pb in segnitite) as described above, whereas the inward tilting of the same apices in pyrochlore provides octahedral sites for small *M* cations. The large cations in pyrochlore occupy the centers of the six-membered rings as shown in Figure 2b and have hexagonal bipyramidal coordination. New oxide pyrochlore-group phases have recently been reported with compositions close to $[Ca_{0.75}Ti_{0.25}]_2TiNbO_7$, in which a quarter of the large cation sites are occupied by Ti atoms (Roth *et al*. 2008). The structure refinements show that the Ti atoms are displaced by ~0.7 Å from the centers of the six-membered rings to take up trigonal bipyramidal coordination, analogous to the Zn atoms in monoclinic $PbZn_{0.5}Fe_3(AsO_4)_2(OH)_6$.

Another feature of monoclinic $PbZn_{0.5}Fe_3(AsO_4)_2(OH)_6$ that has not been observed in related structures is the *ordered* displacement of the Pb atoms from the ideal sites at the centers of the icosahedra. The Pb^{2+} ion has a $6s^2$ lone pair of electrons, and commonly takes up an off-center position in a site to allow for the volume occupied by the lone pair. Such displacements are reported for a number of alunite-related structures with *D* = Pb, for example beudantite, $PbFe_3(SO_4)(AsO_4)(OH)_6$ (Giuseppetti & Tadini 1989), kintoreite, $PbFe_3(PO_4)_2(OH,H_2O)_6$ (Kharisun *et al*. 1997) and plumbogummite, $PbAl_3(PO_4)_2(OH,H_2O)_6$ (Kolitsch *et al*. 1999). However, in each case, the split atom sites obey the $R\bar{3}m$ symmetry, and their center-of-gravity remains at the undisplaced central position. In contrast, in monoclinic $PbZn_{0.5}Fe_3(AsO_4)_2(OH)_6$, the centers-of-gravity of the multiply-split Pb atom sites are displaced in an ordered way from the ideal sites, in response to the ordering of Zn atoms in half of the available six-membered rings.

Why does monoclinic $PbZn_{0.5}Fe_3(AsO_4)_2(OH)_6$ have divalent cations ordered in the six-membered rings? To help explain this question, it is worth recalling that the alunite-type formulation for segnitite as $PbFe_3(AsO_4)_2(OH)_6$ has a charge imbalance of –1. In the original description of segnitite (Birch *et al*. 1992), the simplified formula was written as $PbFe_3H(AsO_4)_2(OH)_6$, with addition of one H atom to

address this charge imbalance. The apical anions of the AsO_4 tetrahedra in segnitite have a formal (Pauling) valence of 1.25. Birch *et al*. (1992) considered that the most likely location of the extra proton was as apical OH groups, disordered over the two tetrahedra, $AsO_3[O_{0.5}(OH)_{0.5}]$. Since the apical anions of the tetrahedra sit ~1.6 Å above and below the six-membered rings, an alternative way for the structure to meet its valence requirements is to have a low-valence cation equidistant from the two anions. The Zn^{2+} cations meet this requirement and at the same time have a location within the six-membered rings that meets their own bonding and valence requirements. However, since the charge imbalance is only –1 per two tetrahedra, then only 0.5 Zn^{2+} per formula unit is required. In monoclinic $PbZn_{0.5}Fe_3(AsO_4)_2(OH)_6$, this leads to ordering of zinc over half the available six-membered rings. The actual composition has less than 0.5 Zn per formula unit. Divalent ions Cu^{2+} and Fe^{2+} may also occupy the Zn sites to make up the shortfall, although it is also possible that incomplete occupancy of the Zn sites is accompanied by some protonation of the apical oxygen atoms of the tetrahedra to achieve charge balance. It is interesting to speculate that a small monovalent cation such as Li^+ could meet the valence requirements of all the tetrahedron apices by occupying all six-membered rings.

Acknowledgements

The authors thank Ludmilla Malishev and Nick Wilson for help with the electron-microprobe analyses. Thanks to Craig Forsyth at the Chemistry Department of Monash University for the collection of intensity data. We appreciate the helpful and constructive comments of two referees.

References

Bindi, L. & Evain, M. (2007): Gram–Charlier development of the atomic displacement factors into mineral structures: the case of samsonite, $Ag_4MnSb_2S_6$. *Am. Mineral*. **92**, 886-891.

Birch, W.D., Pring, A. & Gatehouse, B.M. (1992): Segnitite, $PbFe_3H(AsO_4)_2(OH)_6$, a new mineral in the lusingite group, from Broken Hill, New South Wales, Australia. *Am. Mineral*. **77**, 656-659.

Birch, W.D. & van der Heyden, A. (1997): Minerals from the Kintore and Block 14 open cuts at Broken Hill, New South Wales. *Aust. J. Mineral*. **3**, 23-71.

Coelho, A.A., Cheary, R.W. & Smith, K.L. (1997): Analysis and structural determination of Nd-substituted zirconolite-4*M*. *J. Solid State Chem*. **129**, 346-359.

Dzikowski, T.J., Groat, L.A. & Jambor, J.L. (2006): The symmetry and crystal structure of gorceixite, $BaAl_3[PO_3(O,OH)]_2(OH)_6$, a member of the alunite supergroup. *Can. Mineral*. **44**, 951-958.

Farrugia, L.J. (1999): WinGX suite for small-molecule single-crystal crystallography. *J. Appl. Crystallogr*. **32**, 837-838.

Foshag, W.F. (1937): Carminite and associated minerals from Mapimi, Mexico. *Am. Mineral*. **22**, 479-484.

Gatehouse, B.M., Grey, I.E., Hill, R.J. & Rossell, H.J. (1981): Zirconolite, $CaZr_xTi_{3-x}O_7$; structure refinements for near-end-member compositions with $x = 0.85$ and 1.30. *Acta Crystallogr*. **B37**, 306-312.

Giuseppetti, G. & Tadini, C. (1989): Beudantite: $PbFe_3(SO_4)(AsO_4)(OH)_6$, its crystal structure, tetrahedral site disordering and scattered Pb distribution. *Neues Jahrb. Mineral., Monatsh*., 27-33.

Goreaud, M. & Raveau, B. (1980): Alunite and crandallite: a structure derived from that of pyrochlore. *Am. Mineral*. **65**, 953-956.

Grey, I.E., Mumme, W.G., Ness, T.J., Roth, R.S. & Smith, K.L. (2003b): Structural relations between weberite and zirconolite polytypes – refinements of doped 3T and 4M $Ca_2Ta_2O_7$ and 3T $CaZrTi_2O_7$. *J. Solid State Chem*. **174**, 285-295.

Grey, I.E., Mumme, W.G., Pekov, I.V. & Pushcharovsky, D. Yu. (2003a): The crystal structure of chromium kassite from the Saranovskoye deposit, northern Urals, Russia. *Am. Mineral*. **88**, 1331-1335.

Jambor, J.L. (1999): Nomenclature of the alunite supergroup. *Can. Mineral*. **37**, 1323-1341.

Jambor, J.L., Owens, D.R., Grice, J.D. & Feinglos, M.N. (1996): Gallobeudantite, $PbGa_3[(AsO_4),(SO_4)]_2(OH)_6$, a new mineral species from Tsumeb, Namibia, and associated new gallium analogues of the alunite–jarosite family. *Can. Mineral*. **34**, 1305-1315.

Kharisun, Taylor, M.R., Bevan, D.J.M. & Pring, A. (1997): The crystal structure of kintoreite, $PbFe_3(PO_4)_2(OH,H_2O)_6$. *Mineral. Mag*. **61**, 123-129.

Kolitsch, U., Tiekink, E.R.T., Slade, P.G., Taylor, M.R. & Pring, A. (1999): Hinsdalite and plumbogummite, their atomic arrangements and disordered lead sites. *Eur. J. Mineral*. **11**, 513-520.

Kuhs, W.F. (1992): Generalised atomic displacements in crystallographic structure analysis. *Acta Crystallogr*. **A48**, 80-98.

Mazzi, F. & Munno, R. (1983): Calciobetafite (new mineral of the pyrochlore group) and related minerals from Campi Flegrei, Italy; crystal structures of polymignyte and zirkelite: comparison with pyrochlore and zirconolite. *Am. Mineral*. **68**, 262-276.

Menchetti, S. & Sabelli, C. (1976): Crystal chemistry of the alunite series: crystal structure refinement of alunite and synthetic jarosite. *Neues Jahrb. Mineral., Monatsh*., 406-417.

MILLS, S.J. (2007): *The Crystal Chemistry and Geochronology of Secondary Minerals from the Broken Hill Deposit, New South Wales*. Ph.D. thesis, Univ. of Melbourne, Melbourne, Australia.

PETRIČEK, V. & DUŠEK, M. (2000): JANA 2000, *a Crystallographic Computing System*. Institute of Physics, Academy of Sciences of the Czech Republic, Prague, Czech Republic.

RADOSLOVICH, E.W. (1982): Refinement of gorceixite in *Cm*. *Neues Jahrb. Mineral., Monatsh.*, 446-464.

RATTRAY, K.J., TAYLOR, M.R., BEVAN, D.J.M. & PRING, A. (1996): Compositional segregations and solid solution in the lead-dominant alunite-type minerals from Broken Hill, N.S.W. *Mineral. Mag.* **60**, 779-785.

ROTH, R.S., VANDERAH, T.A., BORDET, P., GREY, I.E., MUMME, W.G., CAI, L. & NINO, J.C. (2008): Pyrochlore formation, phase relations, and properties in the $CaO–TiO_2–(Nb,Ta)_2O_5$ systems. *J. Solid State Chem.* **181**, 406-414.

SCOTT, K.M. (1987): Solid solution in, and classification of, gossan-derived members of the alunite–jarosite family, northwest Queensland, Australia, *Am. Mineral.* **72**, 178-187.

SHELDRICK, G.M. (1997): SHELXL–97, *a Program for Crystal Structure Refinement*. University of Göttingen, Göttingen, Germany.

SPEK, A.L. (2003): Single crystal structure validation with the program PLATON. *J. Appl. Crystallogr.* **36**, 7-13.

SZYMAŃSKI, J.T. (1985): The crystal structure of plumbojarosite $Pb[Fe_3(SO_4)_2(OH)_6]_2$. *Can. Mineral.* **23**, 659-668.

TRUEBLOOD, K.N., BÜRGI, H.-B., BURZLAFF, H., DUNITZ, J.D., GRAMACCIOLI, C.M., SCHULZ, H.H., SHMUELI, U. & ABRAHAMS, S.C. (1996): Atomic displacement parameter nomenclature. Report of a subcommittee on atomic displacement parameter nomenclature. *Acta Crystallogr.* **A52**, 770-781.

VAN DER HEYDEN, A. & EDGECOMBE, D.R. (1990): Silver–lead–zinc deposit at South mine, Broken Hill. *In* Geology of the Mineral Deposits of Australia and New Guinea (F.E. Hughes, ed.). The Australasian Institute of Mining and Metallurgy, Melbourne, Australia (1073-1077).

Received March 11, 2008, revised manuscript accepted September 1, 2008.